Journal of the European Ceramic Society 16 (1996) 1337–1343

PII: S0955-2219(96)00066-0
0955-2219/96/$15.00

Microstructure and Flexure Creep Behaviour of SiC-Particle Reinforced Al_2O_3 Matrix Composites

Zhen-Yan Deng, Yu-Feng Zhang, Jian-Lin Shi & Jing-Kun Guo

The State Key Laboratory of High Performance Ceramics and Superfine Microstructure, Shanghai Institute of Ceramics, Chinese Academy of Sciences, Shanghai 200050, People's Republic of China

(Received 26 January 1996; revised version received 22 March 1996; accepted 28 March 1996)

Abstract

The flexure creep behaviour of monolithic Al_2O_3 and 10 vol% SiC-particle reinforced Al_2O_3 matrix composites was investigated in air atmosphere at 1160 to 1400°C and under a stress of 40 to 125 MPa. Two kinds of SiC particles with different particle sizes and oxygen contents were used in the composites, one having an average size of 0·6 μm with 1·7 vol% SiO_2 impurities and the other of average size 2·7 μm with 3·4 vol% SiO_2 impurities. Compared with the creep behaviour of monolithic Al_2O_3 the strain rate of the composites with 0·6 μm SiC particles did not decrease; however, the composites with 2·7 μm SiC particles exhibited excellent creep resistance. Microstructure analysis showed that the Al_2O_3 grains in the composites with 0·6 μm SiC particles were mainly equiaxed with most of the SiC particles lying at the grain boundaries or triple-grain junctions, whereas the grain features of the composites with 2·7 μm SiC particles were irregular and elongated and most of the SiC particles were entrapped into Al_2O_3 matrix grains. It was revealed that the entrapment of 2·7 μm SiC particles into Al_2O_3 matrix grains was related to the high SiO_2 impurity content on SiC particle surfaces, and the change of grain morphology and the good high-temperature oxidation resistance were responsible for the creep resistance increase of the composites with 2·7 μm SiC particles. © 1996 Elsevier Science Limited

1 Introduction

Over the past few years, the high-temperature creep and creep fracture behaviour of monolithic Al_2O_3 have been studied extensively,[1–5] owing to the increasing emphasis on the development of structural ceramics for high-temperature applications. Although Al_2O_3 itself is not suitable as a high-temperature structural material, it is a potential matrix material for some structural composites with high-temperature capability because of the good microstructured stability of Al_2O_3 at high temperature. For example SiC whiskers have been successfully incorporated into Al_2O_3 by many researchers[6–8] and the high-temperature creep resistance of Al_2O_3 was apparently improved. However, SiC whiskers are expensive for practical applications and pose health hazards during material processing. These shortcomings would be overcome if the SiC whiskers could be replaced by cheap SiC particles.

Recently, Niihara[9] has successfully developed Al_2O_3/SiC nanocomposites which were formed by dispersion of nanometre-size SiC particles into Al_2O_3 matrix grains and at grain boundaries. He found that addition of as little as 5 vol% 0·3 μm SiC particles could increase the strength of hot-pressed alumina from 350 MPa to over 1 GPa and the fracture toughness from 3·25 to 4·7 MPa $m^{1/2}$, this high strength being maintained up to 1200°C. Ohji *et al.*[10] subsequently conducted tensile creep tests for Al_2O_3/17 vol% SiC nanocomposites and monolithic Al_2O_3 at 1200 to 1300°C and under a stress of 50 to 150 MPa. They revealed that the minimum creep rate of the nanocomposites was about three orders of magnitude lower and the creep life was 10 times longer than those of the monolithic Al_2O_3. The purpose of this paper is to study the effects of different SiC particles on the morphology and creep properties of SiC-particle reinforced Al_2O_2 matrix composites.

2 Experimental

Highly pure α-Al_2O_3 was obtained by calcining γ-Al_2O_3, with a mean particle size of 1 μm. SiC particles with two different sizes, 0·6 and 2·7 μm, were used in this study; these are represented by S and L in the figures hereafter. The main impurity in the SiC particles was SiO_2: 1·7 and 3·4 vol% SiO_2 in the 0·6 and 2·7 μm SiC particles, respectively. In the composites, 10 vol% SiC particles and 0·5 vol% MgO

were added. The monolithic Al_2O_3 and composites were obtained by hot-pressing under 20 MPa in a flowing Ar atmosphere at 1700°C for 30 min.

The dense monolithic Al_2O_3 and composite tiles were ground and sectioned into $2 \times 4 \times 40$ mm^3 test bars with the edges chamfered for creep experiments. Density measurements performed on the specimens showed that the density of monolithic Al_2O_3 was over 99·9% of theoretical density, and those of the composites with 0·6 μm SiC particles (ASS) and with 2·7 μm SiC particles (ASL) were 99·6 and 99·5% of theoretical density, respectively. The flexure creep tests were conducted in air atmosphere at 1160 to 1400°C under the stress of 40 to 125 MPa. The specimens were loaded in a four-point flexure fixture with inner and outer span lengths of 10 and 30 mm, respectively. The applied stress and resultant strain were calculated using the method described by Cannon *et al.*[1] in the small strain situation. The microstructures of as-received and creep specimens were analysed by scanning electron microscopy (SEM) and transmission electron microscopy (TEM), the samples of creep specimens for TEM observation being cut from the tensile side of the specimen.

3 Creep Results

The creep curves of monolithic Al_2O_3 and composites at 1260°C and 75 MPa are shown in Fig. 1. Apart from the ASS specimen which fractured in the creep test, monolithic Al_2O_3 and ASL specimens were crept to reach minimum strain rate. Compared with the monolithic Al_2O_3, the strain rate of ASS does not decrease, but ASL exhibits excellent creep resistance.

Figure 2 shows stress dependences of steady-state or minimum creep rates for the monolithic Al_2O_3 and composites at T = 1260°C. Apparent linear fitting indicates that the stress exponent of

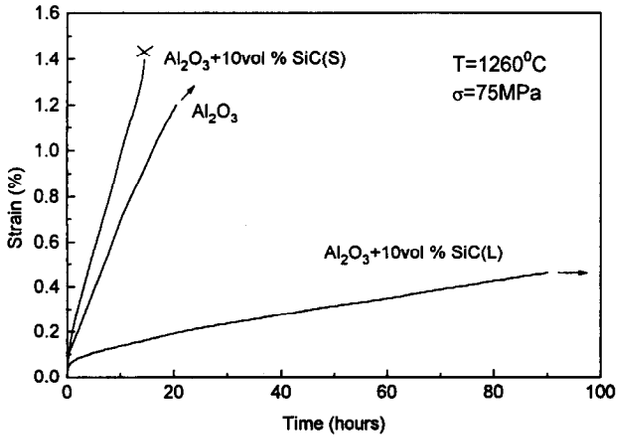

Fig. 1. Flexure creep curves of monolithic Al_2O_3 and composites at 1260°C and 75 MPa, where the ASS specimen fractured in the creep test.

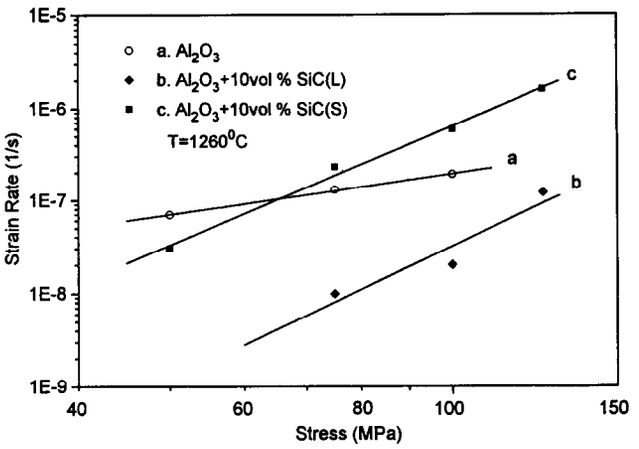

Fig. 2. Stress dependences of steady-state or minimum creep rate for the monolithic Al_2O_3, and composites at 1260°C. The stress exponent for strain rate is 1·45 for monolithic Al_2O_3, 4·27 and 4·75 for ASS and ASL, respectively.

monolithic Al_2O_3 is 1·45, which agrees reasonably well with the results reported by Cannon *et al.*[1] and is smaller than the stress exponent of 2·9 reported for polycrystalline Al_2O_3 prepared by nanometre-sized Al_2O_3 powders.[10] The stress exponents of ASS and ASL are 4·27 and 4·75, respectively, which approach the stress exponents of SiC-whisker reinforced Al_2O_3 matrix composites[11,12] and are larger than the stress exponent of 2·2 for Al_2O_3/SiC nanocomposites.[10] Crudely, the strain rate of ASL is about one order of magnitude lower than those of monolithic Al_2O_3 and ASS. Because the stress exponent of ASS is higher than that of monolithic Al_2O_3, the strain rate of the former is lower than that of the latter at the low stress region and higher than that of the latter at the high stress region. Activation energies of monolithic Al_2O_3 and composites for steady-state or minimum strain rate were obtained from Arrhenius plots by apparent linear regression analysis, as shown in Fig. 3. The activation energy of monolithic Al_2O_3 at 75 MPa is 531 kJ mol^{-1}, which is consistent

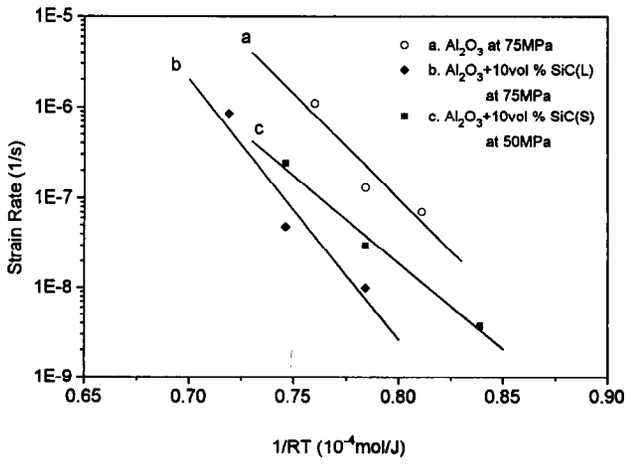

Fig. 3. Arrhenius plots at 75 MPa for monolithic Al_2O_3 and ASL, and at 50 MPa for ASS.

with the results previously reported[1,6] for polycrystalline Al_2O_3. The activation energy of ASS at 50 MPa is 444 kJ mol^{-1}, which is smaller than that of monolithic Al_2O_3. Because the activation energy decreases with the increase in the applied load,[1] the activation energy of ASS at 75 MPa should be smaller than 444 kJ mol^{-1}. On the other hand, the activation energy of ASL at 75 MPa is 666 kJ mol^{-1}, which is larger than that of monolithic Al_2O_3.

4 Discussion

4.1 Al_2O_3 grain morphology

Figure 4 shows the grain morphology of the as-received monolithic Al_2O_3 and composites. In Fig. 4(A) it can be seen that the monolithic Al_2O_3 has a uniform grain-size distribution and equiaxed grain morphology, with an average grain size of about 5 μm. The TEM micrograph of ASS [Fig. 4(B)] indicates that most of the SiC particles are on the grain boundaries or triple-grain junctions (grey particles). In general, the Al_2O_3 matrix grains in ASS have regular equiaxed morphology and the average grain size is smaller than that of monolithic Al_2O_3 due to grain growth suppression by the SiC particles.[13] Occasionally elongated Al_2O_3 grains can also be seen which, as estimated under TEM observation, account for about 10% of the total Al_2O_3 matrix grains, as shown in Fig. 4(B) (indicated by arrow). The features of ASL are significantly different from those of ASS. Figure 4(C) shows that most of the Al_2O_3 matrix grains in ASL are elongated and the grain boundaries are very irregular, their grain sizes being even larger than those of monolithic Al_2O_3. One unexpected observation is that most of the SiC particles in ASL are entrapped into the Al_2O_3 matrix grains, as shown in Fig. 4(D) (grey particles).

4.2 Effects of SiO_2 impurities in hot-pressing process

According to the growth dynamics of ceramic materials,[14] small SiC particles are easy to entrap

Fig. 4. Grain morphology of as-received specimens: (A) SEM micrograph of the fracture surfaces of monolithic Al_2O_3; (B) TEM micrograph of ASS; (C) and (D) TEM micrographs of ASL.

into the Al_2O_3 matrix grains because the force exerted by an inclusion on a grain boundary is proportional to its radius, and the large SiC particles on the grain boundary hinder grain-boundary breakaway and decrease the propensity for second-phase entrapment.[14] So why are the 2·7 μm SiC particles entrapped into Al_2O_3 matrix grains while the 0·6 μm SiC particles are not? The answer may be related to the impurities included in the starting SiC particles, because the SiC particles used in this study have small amounts of SiO_2 impurities. The SiO_2 impurities and MgO additive could form the MgO–Al_2O_3–SiO_2 system liquid phase with the Al_2O_3 matrix during the hot-pressing process.[15] This liquid phase facilitates the dissolution and reprecipitation process of Al and O ions and accelerates Al_2O_3 matrix grain growth. The effects of liquid phase on the grain growth in Al_2O_3 have been studied in detail by Kaysser *et al.*[16] who showed that the liquid phase on the grain boundaries leads to growth anisotropy of Al_2O_3 matrix grains, and an elongated Al_2O_3 grain morphology forms in the Al_2O_3-containing glassy phase. Because the SiO_2 content in 2·7 μm SiC particles (3·4 vol%) is twice that in 0·6 μm SiC particles (1·7 vol%) and the total surface area of the 0·6 μm SiC particles is 4·5 times larger than that of 2·7 μm SiC particles when their volume is the same, the SiO_2 content per unit area on 2·7 μm SiC particle surfaces is about one order of magnitude higher than that on 0·6 μm SiC particle surfaces. The large amount of SiO_2 on 2·7 μm SiC particle surfaces would form a large amount of MgO–Al_2O_3–SiO_2 liquid phase during the hot-pressing process, which could accelerate Al_2O_3 grain growth and grain boundary movement near SiC particles. This is the reason why most of the 2·7 μm SiC particles are entrapped into the Al_2O_3 matrix grains and the 0·6 μm SiC particles are on the grain boundaries. In addition, the elongated grain morphology and irregular grain boundaries in ASL are also related to the liquid phase capping SiC particles in the hot-pressing process. Although the small amount of SiO_2 on 0·6 μm particle surfaces cannot entrap most of the SiC particles into Al_2O_3 matrix grains, small amounts of elongated Al_2O_3 grains (10%) are also seen in their morphology.

4.3 Creep deformation mechanisms and oxidation effects

Grain-boundary diffusion is the most predominant deformation mechanism of polycrystalline Al_2O_3 at temperatures below 1400°C.[7] The stress exponent, 1·45, of monolithic Al_2O_3 shows that grain-boundary sliding without a glassy phase, some accommodated by diffusion and some unaccommodated, is the principal creep mechanism.[1,17] This has been substantiated by TEM observation of the crept monolithic Al_2O_3 sample on the tensile side, as shown in Fig. 5(A), which indicates that large extensive voids exist at triple-grain junctions and grain boundaries on the tensile side of crept monolithic Al_2O_3 specimens formed by unaccommodated grain-boundary sliding. The creep mechanisms in multiphase ceramics cannot be reliably inferred from measured values of activation energies or stress exponents.[7] In our observations, small amounts of cavities have been observed in triple-grain junctions in the two kinds of crept composite specimens, and there is no evidence of dislocation glide in the matrix. We conclude that grain-boundary sliding, some accommodated by diffusion and some unaccommodated, is also the principal creep mechanisms in the composites.[7]

Ohji *et al.*[10] reported that the improvement of creep resistance for Al_2O_3/SiC nanocomposite was due to the pinning effect of the intergranular SiC particles, because the intergranular SiC particles rotated and plunged into the Al_2O_3 grains during the grain-boundary sliding when creep occurred. In our ASS composites, although most of the SiC particles are on the grain boundaries, no apparent improvement of creep resistance is observed. This behaviour can be attributed to the serious oxidation of SiC near particles on the grain boundaries during creep in air, as shown in Fig. 5(B), where most SiC particles near Al_2O_3 grain interfaces have been oxidized (indicated by arrow). The by-product of oxidation reaction is SiO_2, which forms a glassy phase with MgO additive and Al_2O_3 matrix on the grain boundaries. The presence of a viscous amorphous film along interfaces undoubtedly facilitates grain-boundary and interface sliding, decreases the interface bond strength, and decreases the creep resistance of the composites. A layer of glassy phase at the grain boundaries and interfaces would also facilitate Al_2O_3 dissolution–reprecipitation reactions. The MgO–Al_2O_2–SiO_2 glass film along boundaries would permit Al_2O_3 to dissolve and reprecipitate, thus allowing grains to change their shape to accommodate deformation under applied stress, so only a small amount of small cavities existed at triple-grain junctions of crept ASS specimens. Raj and Ashby[18] calculated the sliding rate with diffusional accommodation when secondary particles were present on the grain boundaries and showed that creep was not slowed if the diffusivity of the particle–matrix interface was equivalent to that of the matrix–matrix interface. Although the diffusion ability in the pure SiC–Al_2O_3 interface is significantly lower than that in the Al_2O_3–Al_2O_3 interface[13] as exemplified by the Al_2O_3/SiC nanocomposite,[10] the

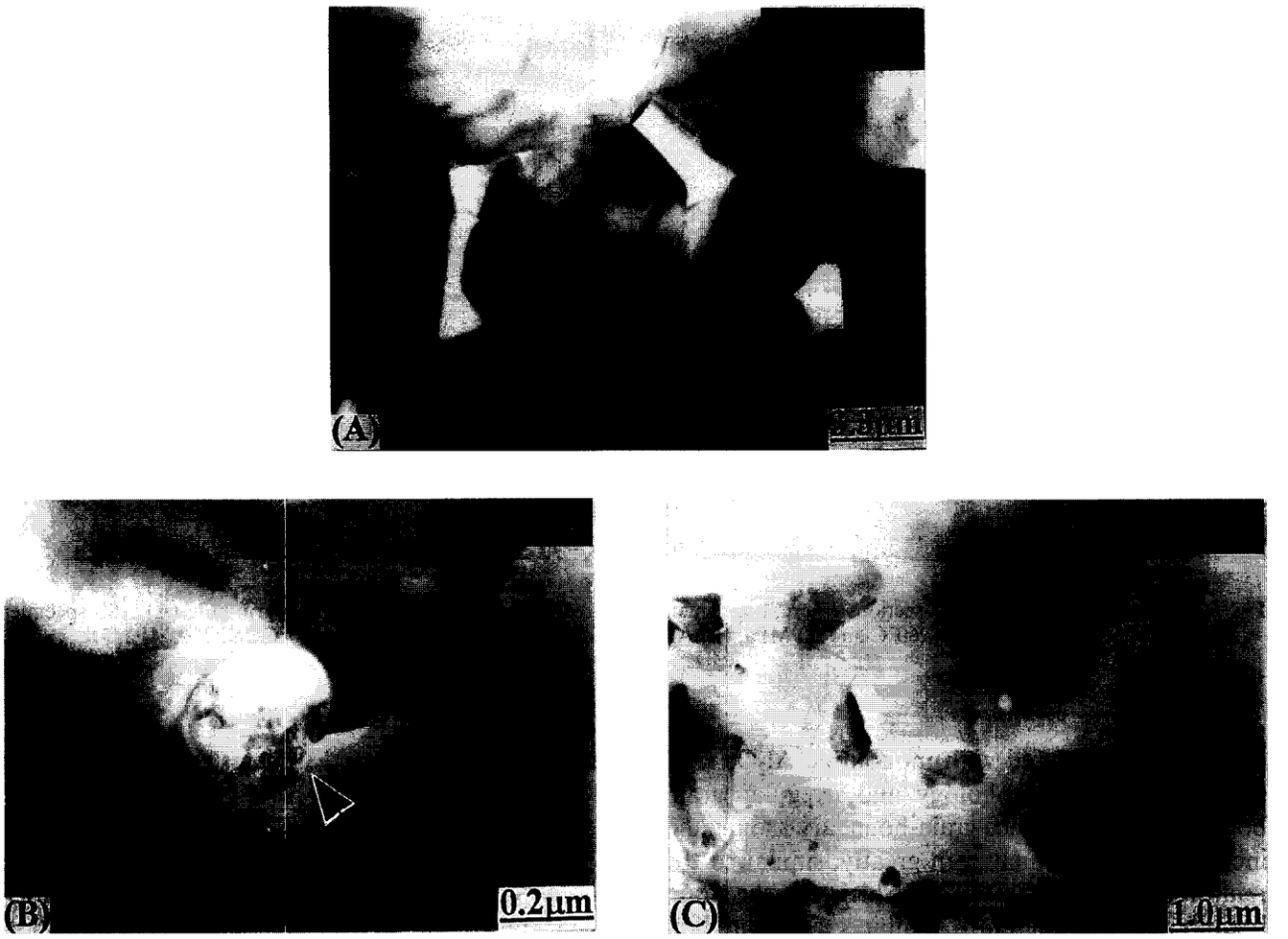

Fig. 5. TEM micrographs of samples taken from the tensile side of crept specimens: (A) monolithic Al_2O_3 crept for 73 h at T = 1260°C and 50 MPa with creep strain of 2·27%; (B) ASS specimen crept for 71 h at T = 1260°C and 50 MPa with creep strain of 1·23%; (C) ASL specimen crept for 88 h at T = 1260°C and 100 MPa with creep strain of 0·53%.

glass phase formed by oxidation reaction along SiC–Al_2O_3 interfaces in our ASS makes the diffusivity of SiC–Al_2O_3 interfaces larger than that of pure Al_2O_3–Al_2O_3 interfaces. These are the reasons why the creep resistance of ASS is not improved compared with that of monolithic Al_2O_3.

The situation in ASL is different from that in ASS, owing to the fact that most of its SiC particles are entrapped into Al_2O_3 matrix. The oxidation reactions for SiC particles inside the Al_2O_3 matrix are not as serious as those for SiC particles on the grain boundaries, because oxygen lattice diffusion in alumina is one order of magnitude lower than that of oxygen grain boundary diffusion.[15] Figure 5(C) shows that the SiC particles inside the Al_2O_3 matrix in ASL have no apparent oxidation after being crept for 88 h at T = 1260°C and 100 MPa. The large difference of oxidation behaviour between the two kinds of composites can also be seen from the surface oxidation layer of crept specimens. Figure 6 shows cross-sections of the crept composite specimens prepared by mechanical fracture and grinding, and indicates that the crept ASS specimen surface has been seriously oxidized, accompanied by carbon monoxide-induced bubbles on its surface layer.[19] The thickness of the surface oxidation layer is about 100 μm, as shown in Fig. 6(A), when the specimen was crept for 71 h in air at T = 1260°C and 50 MPa. The ASL specimen exhibits excellent high-temperature oxidation resistance, as shown in Fig. 6(B), where there is no apparent oxidation layer on the specimen surface after creep testing for 88 h in air at T = 1260°C and 100 MPa. Because of the good oxidation resistance at high temperature, the amount of glass phase on grain boundaries of ASL is much lower. Although 3·4 vol% SiO_2 existed on the starting 2·7 μm SiC particle surfaces, these SiO_2 impurities may be not on the Al_2O_3 grain boundaries due to the SiC particles being entrapped into Al_2O_3 matrix grains.

The lack of glass phase on the Al_2O_3 grain boundaries would enhance the creep resistance of ASL, compared with ASS. The elongated grain morphology and irregular grain boundaries are the main causes for the improved creep resistance

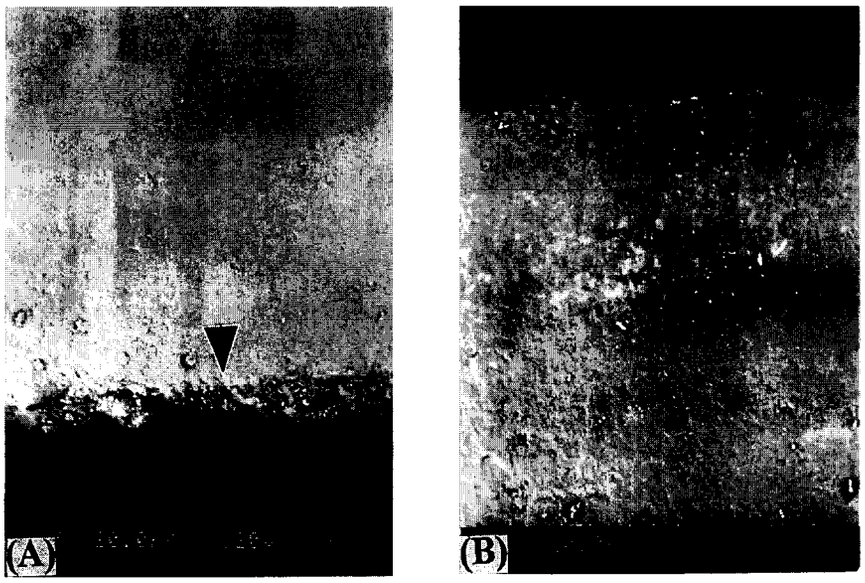

Fig. 6. SEM micrographs of cross-sections of crept specimens prepared by mechanical fracture and grinding: (A) ASS specimen crept for 71 h at $T = 1260°C$ and 50 MPa; (B) ASL specimen crept for 88 h at $T = 1260°C$ and 100 MPa.

of ASL, as compared with monolithic Al_2O_3. The elongated grain morphology and irregular grain boundaries could reduce grain-boundary sliding and increase the diffusional path greatly, similar to the reinforcing effect of whiskers which pin the grain boundaries and therefore inhibit grain-boundary sliding.[6,8] In addition, the small amount of SiC particles on grain boundaries in ASL may also inhibit grain-boundary sliding by pinning grain boundaries[10] and improve the creep resistance of ASL, due to the larger size of SiC particles in ASL. On the other hand, the grain size is a factor affecting creep strain rate,[6,17] but it could account for only a small amount of the difference between monolithic Al_2O_3 and composites.

The different creep behaviours of monolithic Al_2O_3 and composites also reflect the difference in their activation energies. Because of the glass phase along grain boundaries formed by the oxidation reaction in ASS, grain-boundary diffusion becomes easy and the activation energy (444 kJ mol^{-1}) of ASS is smaller than that (531 kJ mol^{-1}) of monolithic Al_2O_3. The high activation energy (666 kJ mol^{-1}) of ASL could be attributable to diffusion being more difficult along the elongated and irregular grain boundaries in ASL than along the equiaxed grain boundaries in monolithic Al_2O_3.

5 Conclusions

We have investigated the flexure creep behaviour of monolithic Al_2O_3 and composites with two kinds of different SiC particles, in air atmosphere at 1160 to 1400°C and under stresses from 40 to 125 MPa. The following results were obtained.

(1) The ASL composites (with 10 vol% 2·7 μm SiC particles) exhibited excellent creep resistance due to their elongated grain morphology, irregular grain boundaries and good oxidation resistance. The creep resistance of ASS (with 10 vol% 0·6 μm SiC particles) was not as good as that of ASL, because of the serious oxidation of the SiC particles on grain boundaries in ASS during creep tests.
(2) Most of the 2·7 μm SiC particles were found to be entrapped into Al_2O_3 matrix grains. This is believed to result from the fact that a high content of SiO_2 impurities existed on 2·7 μm SiC particle surfaces: the SiO_2 formed liquid phase which accelerated the Al_2O_3 grain growth and grain-boundary movement near SiC particles in the hot-pressing process.
(3) Oxidation of the SiC particles on grain boundaries formed thin glass films along grain boundaries in ASS during creep tests, and reduced the activation energy of ASS. The elongated grain morphology and irregular grain boundaries in ASL increased the activation energy of ASL.

Acknowledgement

This work was supported by the Shanghai Postdoctoral Foundation and the Young Scientist Foundation of the Chinese Academy of Sciences.

References

1. Cannon, R. M., Rhodes, W. H. & Heuer, A. H., Plastic deformation of fine-grained alumina (Al_2O_3): I, Interface-controlled diffusional creep. *J. Am. Ceram. Soc.*, **63** (1980) 46–53.
2. Heuer, A. H., Tighe, N. J. & Cannon, R. M., Plastic deformation of fine-grained alumina (Al_2O_3): II, Basal slip and nonaccommodated grain-boundary sliding. *J. Am. Ceram. Soc.*, **63** (1980) 53–58.
3. Robertson, A. G., Wilkinson, D. S. & Càceres, C. H., Creep and creep fracture in hot-pressed alumina. *J. Am. Ceram. Soc.*, **74** (1991) 915–921.
4. Wilkinson, D. S., Càceres, C. H. & Robertson, A. G., Damage and fracture mechanisms during high-temperature creep in hot-pressed alumina. *J. Am. Ceram. Soc.*, **74** (1991) 922–933.
5. Murphy, D., Jakus, K., Ritter, J. E. & Hill, B. C., High-temperature behavior of indent and creep-nucleated cracks in vitreous-bonded alumina. *J. Am. Ceram. Soc.*, **78** (199) 1914–1920.
6. Arellano-López, A. R., Cumbrera, F. L., Domínguez-Rodríguez, A., Goretta, K. C. & Routbort, J. L., Compressive creep of SiC-whisker-reinforced Al_2O_3. *J. Am. Ceram. Soc.*, **73** (1990) 1297–1300.
7. Lipetzky, P., Nutt, S. R., Koester, D. A. & Davis, R. F., Atmospheric effects on compressive creep of SiC-whisker-reinforced alumina. *J. Am. Ceram. Soc.*, **74** (1991) 1240–1247.
8. Arellano-López, A. R., Domínguez-Rodríguez, A., Goretta, K. C. & Routbort, J. L., Plastic deformation mechanisms in SiC-whisker-reinforced alumina. *J. Am. Ceram. Soc.*, **76** (1993) 1425–1432.
9. Niihara, K., New design concept of structural ceramics—ceramic nanocomposites. *J. Ceram. Soc. Jpn*, **99** (1991) 974.
10. Ohji, T., Nakahira, A., Hirano, T. & Niihara, K., Tensile creep behavior of alumina/silicon carbide nanocomposite. *J. Am. Ceram. Soc.*, **77** (1994) 3259–3262.
11. Nutt, S. R., Lipetzky, P. & Becher, P. F., Creep deformation of alumina–SiC composites. *Mater. Sci. Eng.*, **A126** (1990) 165–172.
12. Tuffe, S., Dubois, J., Jorand, Y., Fantozzi, G. & Barbier, G., Processing and fracture behaviour of hot pressed silicon carbide whisker reinforced alumina. *Ceram. Int.*, **20** (1994) 425–432.
13. Stearns, L. C., Zhao, J. H. & Harmer, M. P., Processing and microstructure development in Al_2O_3–SiC 'nanocomposites'. *J. Eur. Ceram. Soc.*, **10** (1992) 473–477.
14. Piciacchio, A., Lee, S. H. & Messing, G. L., Processing and microstructure development in alumina–silicon carbide intragranular particulate composites. *J. Am. Ceram. Soc.*, **77** (1994) 2157–2164.
15. Kingery, W. D., *Introduction to Ceramics*, 2nd edition. Wiley, New York, 1976, p. 307 and 240.
16. Kaysser, W. A., Sprissler, M., Handwerker, C. A. & Blendell, J. E., Effect of a liquid phase on the morphology of grain growth in alumina. *J. Am. Ceram. Soc.*, **70** (1987) 339–343.
17. Cannon, W. R. & Langdon, T. G., Review creep of ceramics: Part 1 Mechanical characteristics. *J. Mater. Sci.*, **18** (1983) 1–50.
18. Raj, R. & Ashby, M. F., Grain boundary sliding and diffusional creep. *Metall. Trans.*, **2** (1971) 1113–1127.
19. Chiu, C. C., Influence of surface oxidation on thermal shock resistance and flexural strength of SiC/Al_2O_3 composites. *J. Mater. Sci.*, **29** (1994) 2078–2082.